# IMPROVING HETEROGENEOUS GRAPH LEARNING WITH WEIGHTED MIXED-CURVATURE PRODUCT MANIFOLD

Tuc Nguyen-Van AI Center FPT Software Hanoi, Vietnam tucnv2@fpt.com Dung D. Le VinUniversity Hanoi, Vietnam dung.ld@vinuni.edu.vn

The-Anh Ta
AI Center
FPT Software
Hanoi, Vietnam
anhtt71@fpt.com

# **ABSTRACT**

In graph representation learning, it is important that the complex geometric structure of the input graph, e.g. hidden relations among nodes, is well captured in embedding space. However, standard Euclidean embedding spaces have a limited capacity in representing graphs of varying structures. A promising candidate for the faithful embedding of data with varying structure is product manifolds of component spaces of different geometries (spherical, hyperbolic, or Euclidean). In this paper, we take a closer look at the structure of product manifold embedding spaces and argue that each component space in a product contributes differently to expressing structures in the input graph, hence should be weighted accordingly. This is different from previous works which consider the roles of different components equally. We then propose WEIGHTED-PM, a data-driven method for learning embedding of heterogeneous graphs in weighted product manifolds. Our method utilizes the topological information of the input graph to automatically determine the weight of each component in product spaces. Extensive experiments on synthetic and real-world graph datasets demonstrate that WEIGHTED-PM is capable of learning better graph representations with lower geometric distortion from input data, and performs better on multiple downstream tasks, such as word similarity learning, top-k recommendation, and knowledge graph embedding. We provide the source of implementation in https://github.com/product\_manifold.

#### 1 Introduction

Representation learning aims to acquire the ability to effectively embed meaningful data into feature spaces Bengio et al. (2013). In traditional representation learning models, Euclidean embedded spaces have been predominantly utilized. However, the uniform geometric structure of Euclidean spaces has certain limitations when it comes to providing accurate representations for various types of structured data, particularly graphs such as tree structures Nickel & Kiela (2017) or circular graphs Wilson et al. (2014). Consequently, there is a growing interest in developing methods that enable the embedding of graph features in non-Euclidean spaces Chami et al. (2019); Topping et al. (2022).

Real-world data frequently exhibit diverse patterns and complex geometries that cannot be adequately captured by the uniform structures of Euclidean embedding spaces. It has been observed that Euclidean spaces are often insufficient for embedding various types of real-world graph data, such as hierarchical structures that induce negative curvature geometry Chami et al. (2020a), or cir-

cle structures Wilson et al. (2014) that require positive curvature geometry. Previous research has demonstrated that using spherical embedding spaces instead of Euclidean ones can result in minimal distortion errors when embedding data with circle and ring structures Wilson et al. (2014); Meng et al. (2019). Moreover, models that solely utilize embedding spaces of a single geometric type often struggle to capture mixed structures effectively. These models tend to produce embedding representations with significant geometric distortion compared to the underlying geometry of the input data Gu et al. (2018). In contrast, approaches employing product spaces composed of components with different geometries have shown promising results in graph representation learning.

**Problem** Current geometric embedding models, as seen in Gu et al. (2018); Skopek et al. (2020); Zhang et al. (2021), typically employ product spaces with equally weighted components. In this setup, the learnable parameters are fitted to the training data samples across all component spaces in a uniform manner. However, we contend that this approach hinders the robustness of models when learning data with diverse geometric structures. Specifically, when the input data predominantly exhibit a particular geometric type compared to others, updating all components equally may not be optimal. Instead, it would be advantageous to assign more emphasis to the dominant geometric type during the parameter update process. This would allow the model to better capture and represent the most prevalent geometric structure in the data.

**Our approach** To address this issue, we introduce a novel data-driven approach that incorporates a scoring mechanism for each component in the product spaces. This scoring mechanism enables the automatic learning of weights for each component based on the geometric structures present in the input data. By considering the specific geometric characteristics of the data, our method allows for the construction of flexible and adaptive product spaces. This includes not only updating the weights of the components but also adjusting the geometric curvatures of the spaces. As a result, our models are capable of effectively capturing and representing the complex geometric structures inherent in the data, leading to improved embedding performance.

**Contributions** We summarize our contribution as follows. Firstly, to the best of our knowledge, this is the first work that considers the structure at each component of product manifold and proposes that each component space contributes differently to expressing various geometric structures in the input graph, hence should be weighted accordingly. Secondly, we propose WEIGHTED-PM, a data-driven method for learning to embed of heterogeneous graphs in *weighted* product manifolds. Thirdly, we conduct extensive experiments on both synthetic and real-world datasets to validate our approach to the various downstream tasks.

#### 2 Related works & Background

The field of machine learning has witnessed a proliferation of works focusing on learning data representations in non-Euclidean spaces, as evidenced by studies such as Liu et al. (2019); Chami et al. (2019); Vinh Tran et al. (2020). However, recent research by Yu & De Sa (2023) has highlighted the computational challenges and numerical instability faced by hyperbolic graph convolution networks, particularly in high-dimensional settings. To address this issue, Yu & De Sa (2023) proposed a random feature mapping technique that utilizes the eigenfunctions of the Laplace operator to approximate an isometry-invariant kernel on hyperbolic space. Another notable approach in this area is CurvGAN Li et al. (2022), which introduces a GAN-based graph representation method that preserves the topological properties of discrete structures by approximating them as continuous Riemannian geometric manifolds. However, these methods primarily focus on a single embedding space and may struggle to effectively capture the underlying structure of the input data.

In contrast, the product of spaces has been shown to possess the capability to achieve higher generalization and effectively capture the intrinsic structures of graphs with mixed geometries Gu et al. (2018). By combining multiple spaces with different geometric characteristics, the product of spaces approach offers improved representation learning and a more comprehensive understanding of complex data structures. While several approaches have explored the use of product spaces, few have addressed the challenges associated with defining and updating the component spaces. One such work, Switch Spaces Zhang et al. (2021), introduces a method that selects a combination of K components from a set of N spaces based on input specifications. It employs a gating mechanism to score and

choose subspace components using pairwise relationships in the training data. However, since entities in a graph are not independent and identically distributed (iid), the component spaces selected based on individual input instances may not effectively capture the overall relationships between nodes in the graph. Consequently, Switch Spaces requires embedding spaces with high dimensions (e.g., 100, 500) to achieve competitive performance in various downstream tasks like knowledge graph embedding and recommendation. Unfortunately, this approach unintentionally sacrifices the advantages offered by non-Euclidean models, which can achieve compactness by requiring smaller dimensions to achieve the same capacity as Euclidean space. In our study, we propose a novel approach that leverages a richer and more robust representation space to capture the diverse geometric structures present in graph data. By enhancing the quality of embeddings, our research complements existing graph-based learning methods and enables more effective representation learning.

Non-Euclidean embedding spaces Non-Euclidean representation learning has emerged as a powerful approach, delivering state-of-the-art performance across diverse tasks. Specifically, hyperbolic space has proven effective in tasks such as network embedding Xu et al. (2022a), recommendation systems Vinh Tran et al. (2020); You et al. (2022), and knowledge graphs Chami et al. (2020c); Cao et al. (2022). On the other hand, spherical space excels in modeling directional similarity and data with cyclical structures Meng et al. (2019); Gu et al. (2018). Each of these spaces possesses unique geometric features, and the selection of an appropriate embedding space should be guided by the inherent structure of the data. By leveraging the most suitable embedding space, we can effectively capture the intrinsic properties and relationships within the data, leading to superior performance across a wide range of applications.

**Product manifold** Product manifolds are constructed by combining embedding spaces with different geometric types, such as Euclidean, hyperbolic, and spherical spaces. In the context of representation learning, the concept of product spaces was introduced in Gu et al. (2018), where each component of the product space has a constant curvature. The curvature of the product space is determined by the sum of curvatures of its individual components Di Giovanni et al. (2022), resulting in a constant curvature overall. This property enables product spaces to capture a wide range of curvatures with lower distortion compared to a single space Gu et al. (2018); Takeuchi et al. (2022). As a result, product spaces are particularly well-suited for real-world data that exhibit mixtures of geometric structures. For example, Skopek et al. (2020) developed a Mixed-curvature Variational Autoencoder, which efficiently trains a VAE with a latent space consisting of a product of constant curvature Riemannian manifolds. Additionally, the heterogeneous structure present in user-item interaction graphs can be effectively learned by utilizing product spaces with different curvature components Xu et al. (2022b).

**Distortion error of embedding** Given metric spaces U and V equipped with distances  $d_U$  and  $d_V$  respectively, an embedding is a continuous and injective mapping  $f:U\to V$ . To evaluate the quality of an embedding, we use the average distortion metric  $D_{\mathrm{avg}}(f)$ , which calculates the average distortion over all pairs of points. Distortion between a pair of points a and b is defined as  $\left|\left(\frac{d_V(f(a),f(b))}{d_U(a,b)}\right)^2-1\right|$ .

### 3 Proposed method: Weighted-PM

In this section, we present our approach to learning the weights between sub-geometries with different curvatures in the product of embedding spaces. Our objective is to ensure that the curvatures of the graph embedding spaces closely match the curvatures of the graph itself. To accomplish this, we introduce a novel gating mechanism that assigns a score to each component space. Motivated from the coarsening approaches Ying et al. (2018); Cai et al. (2021), we designed gating mechanism to leverage the message-passing of information across various regions of the input graph, enabling the extraction of topology information. Our gating mechanism divides the graph into multiple parts, where each sub-graph is predominantly characterized by a specific type of geometry, such as a tree or cycle structure. For example, in a graph consisting of a ring of trees where the tree structure dominates, we assign higher scores to hyperbolic components in the product space compared to spherical components. This choice is made to improve the quality of the embeddings produced. By applying this gating mechanism and adjusting the weights between the different sub-geometries, we aim to

achieve a more accurate representation of the graph's underlying structures, resulting in improved embedding results.

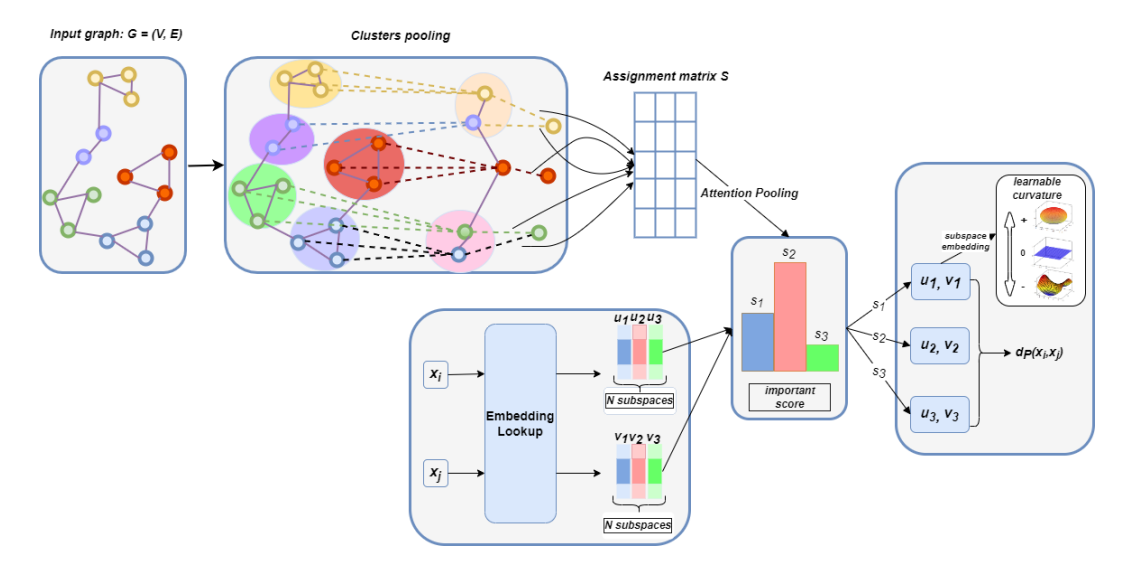


Figure 1: From left to right: for an input graph G=(V,E), we use a hierarchical pooling method to pool G to produce assignment matrices  $S_{n_l \times n_{l+1}}$ , where  $n_{l+1} = N$  is the number of components in the product space; self multi-head attention is then used to capture the weight vector  $\mathbf{s} \in \mathbb{R}^N$  which calculates influence scores among curvatures of subspaces over all the nodes of the input graph G.

**Problem formulation** Given three types of geometry: Euclidean ( $\mathbb{E}$ ), Hyperbolic ( $\mathbb{H}$ ), and Spherical ( $\mathbb{S}$ ). Let  $\mathcal{M}_1, \mathcal{M}_2, \ldots, \mathcal{M}_N$  be N component spaces where  $M_i$  is of one geometric type among  $\{\mathbb{E}, \mathbb{H}, \mathbb{S}\}$ , and dim  $M_i = b_i$ . The goal of our approach is to learn the score  $\mathbf{w} = (w_1, \ldots, w_N) \in \mathbb{R}^N$  from the input graph data on each component of product manifold embedding space in such a way that the embedding of input graph into  $P = w_1 \mathcal{M}_1 \times w_2 \mathcal{M}_2 \times \cdots \times w_N \mathcal{M}_N$  will have lowest possible geometric distortion.

# 3.1 Coarsening input graph data

**Hierarchical pooling layers** Given input graph  $\mathcal{G}$ , with n>0 nodes, adjacency matrix  $\mathbf{A} \in \{0,1\}^{n\times n}$  and node features  $\mathbf{X} \in \mathbf{R}^{n\times d}$ . The matrix  $\mathbf{A}$  represents graph structure:  $\mathbf{A}(i,j)=1$  if there is an edge connecting two nodes i,j, otherwise  $\mathbf{A}(i,j)=0$ . D is the diagonal degree matrix of the graph  $\mathbf{G}$  where  $D_{ii}=\sum_{i}\mathbf{A}_{ij}$ .

We use hierarchical pooling-based GCNs to learn cluster assignments. There are two GCNs with two different sets of parameters in this module. At each layer l, the soft cluster assignment matrix  $\mathbf{S}^{(l)} \in \mathbf{R}^{n_{l-1} \times n_l}$  is computed as follows:

$$\mathbf{S}^{(l)} = \operatorname{softmax}(GNN_1^l(\mathbf{A}^{(l-1)}, \mathbf{X}^{(l-1)})) \text{ with } (\mathbf{A}^{(0)}, \mathbf{X}^{(0)}) = (\mathbf{A}, \mathbf{X}). \tag{1}$$

Then, we apply the second GNN on  $S^{(l)}$  to compute the graph representation at layer l:

$$\mathbf{X}^{(l)} = \mathbf{S}^{(l)}{}^{T} (GNN_{2}^{(l)}(\mathbf{A}^{(l-1)}, \mathbf{X}^{(l-1)})) \text{ and } \mathbf{A}^{(l)} = \mathbf{S}^{(l)}{}^{T} \mathbf{A}^{(l-1)} \mathbf{S}^{(l)}).$$
(2)

Coarsening input graph The hierarchical pooling layer produces a coarsened graph with m < n nodes, a weighted adjacency matrix  $A' \in \mathbb{R}^{m \times m}$ , and node embeddings  $Z' \in \mathbb{R}^{m \times d}$ . This process is then repeated L times, resulting in a GNN model with L layers that operate on the input graph and a series of coarser versions of it. The soft assignment matrix  $S^{(l)}$  assigns each node at layer l to a cluster at the next layer l+1. In other words, each row of  $S^{(l)}$  corresponds to one of the  $n_l$  nodes or clusters at layer l, while each column of  $S^{(l)}$  corresponds to one of the  $n_{l+1}$  clusters at

# Algorithm 1 R-SGD in the product of model spaces

```
1: Initialize x^{(0)} \in \mathcal{P}
 2: for t = 0, ..., T - 1 do
           h \leftarrow \Delta \mathcal{L}_{distortion}(x^{(t)})
 3:
 4:
           Step: Project positive curvature embedding to the tangent space.
 5:
          for i = 1, ..., m do
              v_j \leftarrow \operatorname{proj}_{x^{(t)}}^S(h_i)
 6:
 7:
 8:
           Step: Project negative curvature embedding to the tangent space.
           \begin{aligned} & \textbf{for i} = \mathbf{m} + 1, \dots, \mathbf{m} + \mathbf{n} \ \mathbf{do} \\ & v_i \leftarrow \operatorname{proj}_{x_i^{(t)}}^H(h_i) \end{aligned} 
 9:
10:
11:
12:
           end for
13:
           Step: Euclidean space.
14:
           v_{m+n+1} \leftarrow h_{m+n+1}
15:
           for i = 1, ..., m do
              v_j \leftarrow \operatorname{proj}_{x^{(t)}}^S(h_i)
16:
17:
           end for
           Step: Curvature-wise concatenation.
18:
19:
           v_{m+n+1} \leftarrow h_{m+n+1}
           Step: Project from tangent space to the manifold.
20:
           \begin{aligned} & \textbf{for i} = 1, \dots, m + n + 1 \ \textbf{do} \\ & x_i^{(t+1)} \leftarrow \operatorname{Exp}_{x_i^{(t)}}(v_i) \end{aligned} 
21:
22:
23:
           end for
24: end for
25: return x^{(T)}
```

layer l+1. In our approach, we treat the number of clusters as a hyperparameter and set  $n_{l+1} = N$ , where N is the number of components in the product space P. Each row of  $S^{(l)}$  shows the degree of membership of a node to each component space in P.

**Attention pooling** We use the attention mechanism with the input being the matrix  $\mathbf{S}^{(l)}$  to take the influence vector for each subspace. Consider the matrix  $\mathbf{S}$  in form  $\mathbf{S} = [\mathbf{h}_1, \mathbf{h}_2, ..., \mathbf{h}_N]$ , with  $\mathbf{h}_t \in \mathbb{R}^d$ , and a trainable matrix  $\mathbf{U} \in \mathbb{R}^d$ .

Self attention: We define a relevant scalar weight for each element of the sequence through a softmax layer as follows  $w_t = \operatorname{softmax}(\mathbf{h}_t^T\mathbf{U})$ . Given the set of weights over all the elements of the sequence, we can then obtain the pooled representation as the weighted average of the hidden states  $\mathbf{s} = \sum_{t=1}^{N} \mathbf{h}_t^T \mathbf{w}_t$ .

Multi-head self attention: Considering a number of k heads for the multi-head attention,  $\mathbf{h}_t = [\mathbf{h}_{t1}, \mathbf{h}_{t2}, \ldots, \mathbf{h}_{tk}]$  where  $\mathbf{h}_{tj} \in \mathbb{R}^{d/k}$  and size of each head is d/k. In the same sense, we have a trainable parameter  $\mathbf{U} = [\mathbf{u}_1 \mathbf{u}_2 \ldots \mathbf{u}_k]$  where  $\mathbf{u}_j \in \mathbb{R}^{d/k}$ . Different attention is then applied over each head of the encoded sequence softmax function following  $w_t = \operatorname{softmax}(\mathbf{h}_{tj}^T \mathbf{u}_j)$ , where  $w_{tj}$  corresponds to the attention weight of the head j on the element t. A soft weight representation for each subspace is computed as follows:

$$s_j = \sum_{t=1}^N \mathbf{h}_{tj}^T \mathbf{w}_{tj}.$$
 (3)

This method allows a multi-head self-attention network extracts different kinds of information over different regions of the self-attention network. In the end,  $\mathbf{s} \in \mathbb{R}^N$  represents the average weight of N component spaces in the product manifold P over the  $n_l$  clusters.

## 3.2 Objective function

Let  $\mathbf{s} \in \mathbb{R}^N$  be the weight vector of N components based on the data's local geometry information. The distance between  $x_i, x_j \in P$  is computed following  $d_P^2(x_i, x_j) = \sum\limits_{k=1}^N \mathbf{s}_k \operatorname{dist}^2(x_i^k, x_j^k)$ . Then the base objective  $\mathcal{L}_{base}$  is defined as:

$$\mathcal{L}_{base} = \sum_{1 \le i < j \le n} \left| \left( \frac{d_P(x_i, x_j)}{d_G(X_i, X_j)} \right)^2 - 1 \right| \tag{4}$$

Finally, the total average distortion objective function is defined as  $\mathcal{L} = \mathcal{L}_{base} + \mathcal{L}_{aux}$ , where  $\mathcal{L}_{aux} = \mathcal{L}_{LP} + \mathcal{L}_e$  is a combination of the link prediction loss  $(\mathcal{L}_{LP})$  and the entropy regularization loss  $(\mathcal{L}_e)$ . More precisely,  $\mathcal{L}_{LP} = \left\| \mathbf{A}^{(l)} - \mathbf{S}^{(l)} \mathbf{S}^{(l)^T} \right\|_F$  at each layer l, where  $\| \cdot \|_F$  denotes the

Frobenius norm; and  $\mathcal{L}_e = \frac{1}{n} \sum_{i=1}^n H(\mathbf{S}_i)$  where  $H(\mathbf{S}_i)$  is the entropy of the row  $i^{th}$  in matrix  $\mathbf{S}$ .

Minimizing  $\mathcal{L}_{LP}$  means enforcing close nodes to be pooled together, while minimizing  $\mathcal{L}_e$  makes the output cluster assignment for each node close to a one-hot vector so that the membership for each cluster is clearly defined. Our total average distortion  $\mathcal{L}$  is optimized with the Algorithm 1.

#### 3.3 PHYSICAL MEANING OF SUBSPACE WEIGHTS

In manifold representation learning, the goal is to embed data into appropriate embedding spaces where the curvature of the embedding matches the curvature of the original data. In the case of a product manifold, each data point is partially embedded in different subspaces with varying curvatures. Our work explores the relationship among the curvatures of all the subspaces and introduces a partial update mechanism for the embedding space based on their respective influence scores. In the importance score box of Model Architecture (Figure 1), if the input data is predominantly characterized by hierarchical structures, the importance score of the hyperbolic embedding component  $(s_2)$  will receive a larger value compared to the others  $(s_1$  and  $s_3)$ . In Algorithm 1, we update the subspaces' curvatures and the embedding itself. The higher the curvature embedding scores, the more effort is required to minimize them. As a result, the negative curvature loss should contribute more to the overall loss, leading to more active updates of the embedding spaces associated with negative curvature compared to the other spaces. This ensures that the embedding adapts to the data's curvature characteristics and effectively captures the underlying structures.

# 4 EXPERIMENTS

This section presents our experimental evaluation of the proposed model's performance across various learning tasks. We begin by evaluating the model's effectiveness in improving graph reconstruction, as described in section 4.1. Following this, we apply our framework to four downstream tasks: recommendation systems, knowledge graph embedding, node classification, as well as graph classification, and word similarity tasks.

#### 4.1 Graph reconstruction

We perform experiments on both synthetic and real-world datasets to evaluate the performance of our proposed model. More information on baselines and metrics is shown in Appendix C.1.

Model performance on synthetic datasets Table 1 shows the average distortion  $(D_{\text{avg}})$  of our model on the three synthetic graphs. When d=3, WEIGHTED-PM achieves  $D_{avg}=0.104$  with the product manifold  $\mathbf{s}_1\mathbb{H}^2\times\mathbf{s}_2\mathbb{S}^1$ . Meanwhile, without any constraints in subspace curvatures (PM Gu et al. (2018)), the distortion measure of  $\mathbb{H}^2\times\mathbb{S}^1$  on the Cycle graph is 0.11. Overall, for all three synthetic graphs, our proposed model improves upon the main contender method PM from Gu et al. (2018) by 5.4%, 16.3%, and 18.6%, respectively (Table 1). Similar trend continues in higher dimension d=5, our proposed method improves upon the baseline by 17.3%, 3.3% and 11.9%, respectively (Table 1).

Table 1: $D_{avq}(\downarrow)$ results on the synthetic data sets with the dimension d equal to 3 and 5 respectively.
$\mathbf{s}_i$ are learnable weights depending on input data.

Method	Models	Cycle	Tree	Mix
PM				
	$\mathbb{H}^2  imes \mathbb{S}^1$	0.110	0.055	0.063
WEIGHTED-PM				
	$\mathbf{s}_1\mathbb{H}^2 imes\mathbf{s}_2\mathbb{S}^1$	0.104	0.051	0.058
		(+5.4%)		
	$\mathbf{s}_1\mathbb{H}^1 imes\mathbf{s}_2\mathbb{S}^2$	0.116	0.046	0.051
			(+16.3%)	(+18.6%)
PM				
	$\mathbb{H}^3  imes \mathbb{S}^2$	0.124	0.06	0.054
	$\mathbb{H}^2 \times \mathbb{S}^3$	0.115	0.07	0.052
	$\mathbb{H}^2 \times \mathbb{S}^2 \times \mathbb{E}$	0.12	0.092	0.047
WEIGHTED-PM				
	$\mathbf{s}_1\mathbb{H}^3  imes \mathbf{s}_2\mathbb{S}^2$	0.102	0.068	0.05
	$\mathbf{s}_1\mathbb{H}^2 imes\mathbf{s}_2\mathbb{S}^3$	0.11	0.058	0.054
			(+3.3%)	
	$\mathbf{s}_1\mathbb{H}^2  imes \mathbf{s}_2\mathbb{S}^2  imes \mathbf{s}_3\mathbb{E}$	0.095	0.086	0.041
		(+17.3%)		(+11.9%)

Model performance on benchmark datasets We first employ a single space to generate embedding representations for each dataset in order to explore its intrinsic geometry. Based on these observations, we develop heuristics for the dataset characteristics and utilize them to select the component in the model space product. Then, the learning process optimizes the curvature of each subspace according to the dominant graph structure. Figure 2 presents the average distortion  $D_{\rm avg}$  of embeddings into single model spaces for three complex benchmark datasets, as the number of embedding dimensions increases within the range of [5,100]. We can see that, with the Cs PhDs and Power dataset,  $D_{\rm avg}$  is smaller in hyperbolic space than in spherical space when d < 50, indicating that the hyperbolic space should be considered in the general product space. Similarly, the Cities dataset exhibits a more spherical structure than other geometric properties, and thus components of positive curvature should be used.

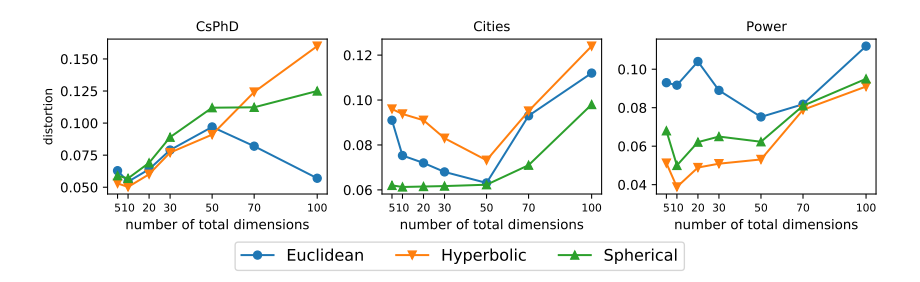


Figure 2: Embedding benchmark datasets on one single space with the number of dimensions increasing gradually.

Table 2 reports the performance of our model on the benchmark datasets. Unlike the results obtained from the synthetic dataset, the best results are predominantly obtained when learning with the product manifolds. This phenomenon is attributed to the more complex structure of real-world data compared to synthetic ones. Specifically, the Power graph dataset has a hierarchical and cyclical structure that can be embedded effectively into any space with a hyperbolic and spherical component. Our proposed model outperforms the main baseline PM Gu et al. (2018) in all cases. With embedding dimension d=10, our model achieves the best distortion on the three datasets. Specifically, in the Cs PhDs dataset, the percentage of improvements in terms of  $D_{\rm avg}$  is 15.6%. In the Power dataset, with the soft gating mechanism, our model achieves better distortion upon the product of the space model with 28.4%. In case d=50, the same improvement with d=50, for specific, these average distortions ( $D_{\rm avg}$ ) compare with the uniform product of spaces (PM) of Gu et al. (2018) is 19.3% and 13.9%, respectively.

Furthermore, Table 2 shows that for distortion of 0.0231 in the product space  $\mathbb{H}^5 \times \mathbb{S}^5$  with the Power dataset, our method determines that the optimally weighted product manifold for embedding the dataset are  $0.83\,\mathbb{H}^5 \times 0.16\,\mathbb{S}^5$ . The ratio between the hyperbolic and spherical components is approximately 5:1, indicating the greater importance of hyperbolic components compared to spherical ones. In contrast, the uniform product embedding space PM of Gu et al. (2018) assumes that each component space contributes equally to learning representations in the product of spaces.

Our method WEIGHTED-PM, on the other hand, captures the constraints relation among all subgeometries of different curvatures in the product manifold, depending on the geometry of the input graph data, leading to better performance than using the uniform product of spaces (PM) without scoring mechanism. Our proposed method has advantages in discovering general models with suitable geometry in the product manifold. Notably, we also observe that the mAP measures are not consistently better than the uniform product model spaces Gu et al. (2018) when  $D_{\rm avg}$  decreases.

Table 2: Average distortion  $D_{\text{avg}}(\downarrow)$  and mAP  $(\uparrow)$  on CsPhDs and Power datasets on dimensions 10 and 50 respectively. The best  $D_{\text{avg}}$  results are in boldface, while the second best results are underlined.

Method	Models	Cs P	Cs PhDs Power		ver
		$D_{avg}$	mAP	$D_{avg}$	mAP
PM	$(\mathbb{H}^2)^5$	0.0357	0.9694	0.0396	0.8739
	$\mathbb{H}^5 imes\mathbb{S}^5$	0.0529	0.9041	0.0323	0.8850
WEIGHTED-PM					
	$\mathbf{s}(\mathbb{H}^2)^5$	0.0301	0.9699	0.0423	0.8540
		(+15.6%)			
	$\mathbf{s}_1\mathbb{H}^5 imes\mathbf{s}_2\mathbb{S}^5$	0.0494	0.9231	0.0231	0.8842
				(+28.4%)	
PM					
	$(\mathbb{H}^5)^{10}$	0.0786	0.8600	0.0723	0.842
	$(\mathbb{H}^{5})^{10}$ $(\mathbb{H}^{10})^{3} \times (\mathbb{S}^{10})^{2}$ $(\mathbb{H}^{10})^{2} \times (\mathbb{S}^{10})^{2} \times \mathbb{E}^{10}$	0.0620	0.9120	0.0510	0.8500
	$(\mathbb{H}^{10})^2 \times (\mathbb{S}^{10})^2 \times \mathbb{E}^{10}$	0.0571	0.9071	0.0495	0.8561
WEIGHTED-PM					
	$rac{\mathbf{s}(\mathbb{H}^5)^{10}}{\mathbf{s_1}(\mathbb{H}^{10})^3  imes \mathbf{s_2}(\mathbb{S}^{10})^2}$	0.0591	0.8900	0.0503	0.8570
	$\mathbf{s_1}(\mathbb{H}^{10})^3  imes \mathbf{s_2}(\mathbb{S}^{10})^2$	0.0590	0.9312	0.0426	0.8620
				(+13.9%)	
	$\mathbf{s_1}(\mathbb{H}^{10})^2 \times \mathbf{s_2}(\mathbb{S}^{10})^2 \times \mathbf{s_3}\mathbb{E}^{10}$	0.0460	0.9240	0.0502	0.8600
		(+19.3%)			

#### 4.2 WEIGHTED-PM ON KNOWLEDGE GRAPH EMBEDDING

Knowledge graphs (KGs) are a fundamental tool for representing information and have a wide range of applications, including question answering and web search Ji et al. (2021). However, KGs are often highly incomplete, which poses a significant challenge for downstream use. The goal of our approach is to address this issue by inferring missing facts in the KGs using entity and relation embedding techniques to map them to appropriate spaces. In this section, we propose using the product of manifolds with a gating mechanism to represent the relations between entities in the KGs. Detailed experimental scenario is shown in Appendix C.3.

**Model performance** Table 3 reports the performance of various methods on two knowledge graphs. To enable a fair comparison, we set the total embedding dimension to 64, which is a common practice in non-Euclidean embedding due to its ability to provide more compact spaces than Euclidean embeddings. Our proposed model achieves superior performance over the baselines on the knowledge embedding graph, highlighting its effectiveness in learning informative representations of the data.

#### 4.3 WEIGHTED-PM ON NODE CLASSIFICATION AND LINK PREDICTION

In this section, we evaluate the performance of our proposed model on node and graph classification tasks. Hyperbolic GCN Chami et al. (2019) uses message-passing on the hyperbolic tangent space for graph convolutional networks (GCNs). However, our proposed model replaces the hyperbolic space with WEIGHTED-PM and applies message passing in the tangent of the product spaces. We

Table 3: Model performance on knowledge graph embedding task. The best results are in boldface, while the second-best results are underlined.

Best model	FB15k-237		WN	18RR
	MRR (†)	HR@3 (↑)	MRR (†)	HR@3 (↑)
RotatE $(E^{64})$	0.228	0.265	0.216	0.384
RotatH $(H^{64})$	0.292	0.320	0.340	0.421
Product-RotatH $((H^{16})^4)$	0.321	0.332	0.352	0.451
SwisE	0.334	0.337	0.378	0.462
WEIGHTED-PM-Rotat	0.339	0.345	0.392	0.469

further introduce  $\delta$  Bridson & Haefliger (2013) which is used to evaluate the degree of tree-likeness of a graph by evaluating its graph distance metric. The value of  $\delta$  ranges from 0 to half of the graph diameter, with trees having  $\delta=0$ , while "circle graphs" and "grid graphs" have a larger  $\delta$ , approximately half of their diameters. Further details on the metrics, datasets, and baselines used in our experiments can be found in Appendix C.4.

**Model performance** Table 4 presents the F1 and AUC scores for the link prediction and node classification tasks. Notably, the DISEASE and AIRPORT datasets exhibit high hyperbolicity ( $\delta$  = 0 and 1, respectively), where the performance of using the product of hyperbolic space surpasses that of using the product of mixture curvatures. This is because the unified product of curvature fails to differentiate the primary intrinsic graph structure and instead adapts equally to spaces that do not align with the graph's topology. Our proposed extension addresses this issue by incorporating a weighting mechanism that identifies the dominant embedding manifold most influenced by the underlying structure of the graph data, leading to improved results in both link prediction and node classification for these two datasets.

Table 4: F1 ( $\uparrow$ ) and AUC ( $\uparrow$ ) scores on DISEASE and AIRPORT datasets. The best results are in boldface, while the second-best results are underlined.

Model	DISEASE AIRPOR		PORT	
	F1	AUC	F1	AUC
$MLP(E^{16})$	$28.8 \pm 2.5$	$72.6 \pm 0.6$	$68.6 \pm 0.6$	$89.8 \pm 0.5$
$MLP(H^{16})$	$41.0\pm1.8$	$75.1 \pm 0.3$	$80.5 \pm 0.5$	$90.8 \pm 0.2$
HGCN Chami et al. $(2019) (H^{16})$	$74.5 \pm 0.9$	$90.8 \pm 0.3$	$90.6 \pm 0.2$	$96.4 \pm 0.1$
Product-HGCN Takeuchi et al. (2022) $(H^8 \times H^8)$	$74.9 \pm 0.6$	$91.1 \pm 0.2$	$90.5 \pm 0.1$	$95.7 \pm 0.2$
Mix-GCN Gu et al. (2018) $(H^5 \times S^5 \times E^6)$	$74.1 \pm 0.3$	$90.8 \pm 0.1$	$90.1 \pm 0.2$	$95.3 \pm 0.1$
Ours $(H^5 \times S^5 \times E^6)$	$\textbf{75.4} \pm \textbf{0.4}$	$\textbf{93.6} \pm \textbf{0.2}$	$\textbf{93.0} \pm \textbf{0.1}$	$\textbf{97.6} \pm \textbf{0.2}$

#### 4.4 WEIGHTED-PM ON RECOMMENDATION SYSTEMS

In this section, we evaluate the performance of our proposed model on the recommendation task. Specifically, we apply WEIGHTED-PM to replace the hyperbolic space in metric learning recommendation (HyperML Vinh Tran et al. (2020)). Detailed information on baselines, datasets and metrics can be seen in Appendix C.2.

**Objective function** In HyperML Vinh Tran et al. (2020), the push-pull loss is proposed to learn the metric between the positive and negative items. The overall objective is defined as  $\mathcal{L} = \mathcal{L}_P + \gamma \mathcal{L}_D$ , where pull-push loss  $\mathcal{L}_P$  and distortion loss  $\mathcal{L}_D$  are defined as:

$$\mathcal{L}_{P} = \sum_{(i,j)\in\mathbb{S}} \sum_{(i,k)\notin\mathbb{S}} [m + d_{\mathbb{D}}^{2}(i,j) - d_{\mathbb{D}}^{2}(i,k)]_{+}, \tag{5}$$

$$\mathcal{L}_{D} = \sum_{(i,j)\in\mathbb{S}} \left[ \frac{d_{\mathbb{D}}(f(i),f(j)) - d_{\mathbb{E}}(i,j)|}{d_{\mathbb{E}}(i,j)} \right]_{+} + \sum_{(i,k)\notin\mathbb{S}} \left[ \frac{d_{\mathbb{D}}(f(i),f(k)) - d_{\mathbb{E}}(i,k)}{d_{\mathbb{E}}(i,k)} \right]_{+}, \tag{6}$$

where  $|z|_+ = \max(0, z)$ , m > 0 is the margin size (m = 0.4 in this paper), and f(.) is a mapping function  $f: \mathbb{E} \to \mathbb{D}$  (f is the identity in Vinh Tran et al. (2020)),  $\gamma$  is the multi-task learning weight and  $\mathbb{S}$  is the set of positive user-item pairs. We use the same loss function in Vinh Tran et al.

(2020) with a difference in the distance on  $\mathbb{D}$ . For specific, we compute the distance d between two embeddings in the product of model spaces.

Table 5:  $H@10(\uparrow)$  and  $N@10(\uparrow)$  results of on the

MovieLens 1M and LastFM-20K datasets with di-Table 6 mension d are 32 and 64 respectively.

Model	Movi	eLens	Last	tFM
	H@10	N@10	H@10	N@10
	0.641	0.420	0.171	0.113
	0.655	0.435	0.173	0.123
$(\mathbb{H}^{8})^{4}$	0.702	0.473	0.190	0.136
$(\mathbb{H}^{16})^2$	0.682	0.465	0.180	0.129
$\mathbf{s}(\mathbb{H}^8)^4$	0.710	0.483	0.193	0.140
$\mathbf{s}(\mathbb{H}^{16})^2$	0.672	0.460	0.180	0.129
	0.721	0.513	0.163	0.098
11.11	0.739	0.520	0.166	0.101
$(\mathbb{H}^{16})^4$	0.740	0.520	0.182	0.110
$(\mathbb{H}^{32})^2$	0.750	0.521	0.172	0.105
$\mathbf{s}(\mathbb{H}^{16})^4$	0.732	0.496	0.180	0.108
$\mathbf{s}(\mathbb{H}^{32})^2$	0.752	0.522	0.169	0.101
	$\begin{array}{c} \mathbb{E}^{32} \\ \mathbb{H}^{32} \\ (\mathbb{H}^8)^4 \\ (\mathbb{H}^{16})^2 \\ \mathbf{s}(\mathbb{H}^8)^4 \\ \\ \mathbf{s}(\mathbb{H}^{16})^2 \\ \mathbb{E}^{64} \\ \mathbb{H}^{64} \\ (\mathbb{H}^{16})^4 \\ (\mathbb{H}^{32})^2 \\ \mathbf{s}(\mathbb{H}^{16})^4 \end{array}$	$\begin{array}{ccc} & \text{H@ 10} \\ \mathbb{E}^{32} & 0.641 \\ \mathbb{H}^{32} & 0.655 \\ (\mathbb{H}^8)^4 & 0.702 \\ (\mathbb{H}^{16})^2 & 0.682 \\ \mathbf{s}(\mathbb{H}^8)^4 & \textbf{0.710} \\ \mathbf{s}(\mathbb{H}^{16})^2 & 0.672 \\ \mathbb{E}^{64} & 0.721 \\ \mathbb{H}^{64} & 0.739 \\ (\mathbb{H}^{16})^4 & 0.740 \\ (\mathbb{H}^{32})^2 & 0.750 \\ \mathbf{s}(\mathbb{H}^{16})^4 & 0.732 \\ \end{array}$	$\begin{array}{c cccc} & \text{H@10} & \text{N@10} \\ \mathbb{E}^{32} & 0.641 & 0.420 \\ \mathbb{H}^{32} & 0.655 & 0.435 \\ (\mathbb{H}^8)^4 & 0.702 & 0.473 \\ \hline (\mathbb{H}^8)^2 & 0.682 & 0.465 \\ \mathbf{s}(\mathbb{H}^8)^4 & 0.710 & 0.483 \\ \mathbf{s}(\mathbb{H}^{16})^2 & 0.672 & 0.460 \\ \hline \mathbb{E}^{64} & 0.721 & 0.513 \\ \mathbb{H}^{64} & 0.739 & 0.520 \\ (\mathbb{H}^{16})^4 & 0.740 & 0.520 \\ \hline (\mathbb{H}^{32})^2 & 0.750 & 0.521 \\ \mathbf{s}(\mathbb{H}^{16})^4 & 0.732 & 0.496 \\ \hline \end{array}$	$\begin{array}{c ccccc} & H@10 & N@10 & H@10 \\ E32 & 0.641 & 0.420 & 0.171 \\ H32 & 0.655 & 0.435 & 0.173 \\ (H8)^4 & 0.702 & 0.473 & 0.190 \\ (E1)^2 & 0.682 & 0.465 & 0.180 \\ S(H8)^4 & 0.710 & 0.483 & 0.193 \\ \hline S(H16)^2 & 0.672 & 0.460 & 0.180 \\ E64 & 0.721 & 0.513 & 0.163 \\ H64 & 0.739 & 0.520 & 0.166 \\ (H16)^4 & 0.740 & 0.520 & 0.182 \\ \hline (H32)^2 & 0.750 & 0.521 & 0.172 \\ S(H16)^4 & 0.732 & 0.496 & 0.180 \\ \hline \end{array}$

<sup>1</sup> -Table 6: Spearman rank correlation (↑) on the
WS-353 dataset on the weighted product mani-
fold with 10 and 50 dimensions, respectively.

Method	Best model	Spearman rank
Single	$\mathbb{H}^{10}$	0.4412
PM	$\mathbb{H}^5 \times \mathbb{H}^5$	0.4489
WEIGHTED-PM	$\mathbf{s}_1\mathbb{H}^5\times\mathbf{s}_2\mathbb{H}^5$	0.4510
Single	$\mathbb{H}^{50}$	0.6389
PM	$(\mathbb{H}^{25})^2$	0.6421
	$(\mathbb{H}^{10})^5$	0.6531
WEIGHTED-PM	$\mathbf{s}_1\mathbb{H}^{25}\times\mathbf{s}_2\mathbb{H}^{25}$	0.6506
	$\mathbf{s}(\mathbb{H}^{10})^5$	0.6612

**Model performance** Table 5 reports the H@10 and N@10 scores for two different datasets, considering the number of factors  $d \in \{32, 64\}$ . Our experiments demonstrate that, overall, CML and HyperML achieve better results with the weighted product manifolds (WEIGHTED-PM) than in the Hyperbolic space alone, highlighting the advantages of using scoring sub-manifolds to model the distance between users and items.

#### 4.5 Performance on word similarity task

We evaluated our model's performance on applications that require an understanding of the underlying manifold structure. To conduct our experiment, we trained word embeddings on the Word Similarity (WS-353) benchmark dataset, following the methodology established in previous works such as Gu et al. (2018); Leimeister & Wilson (2018). Our implementation is based on hyperbolic skip-gram embeddings from Leimeister & Wilson (2018).

**Setup** For our setup, we utilized the standard skip-gram model Mikolov et al. (2013) and extended the loss function to a generic objective suitable for arbitrary manifolds, using a variant of the objective used in Leimeister & Wilson (2018). Specifically, given a word u and a target w with label y=1 if w is a context word for u and y=0 if it is a negative sample, our model is represented by  $P(y \mid w, u) = \sigma\left((-1)^{1-y}\left(-\cosh\left(d\left(\alpha_u, \gamma_w\right)\right) + \theta\right)\right)$ .

**Word similarity** To measure the effectiveness of our model, we evaluated its performance on the WS-353 dataset using the Spearman rank correlation  $\rho$  between our scores and annotated ratings. We obtained the dataset from Finkelstein et al. (2001), and the results of our experiment are presented in Table 6. Our model outperformed the hyperbolic word embeddings of Leimeister & Wilson (2018) and the product space (PM) in all dimension settings.

#### 5 CONCLUSIONS

Real-world data often possess intricate geometric structures that are challenging to capture by embedding into spaces with uniform curvature. To address this issue, we propose a method that partially extracts the topology information from the input data to update the embedding vectors and curvature of each subspace. Our motivation is that graphs are constructed by combining simple structure topologies, such as trees, cycles, and stars. Our approach introduces a data-driven method of weighted product spaces for learning better representations. Our empirical experiments on synthetic and real-world datasets demonstrate that our framework enhances the embedding quality of input graphs with varying structures and improves the performance of the downstream tasks.

### REFERENCES

- Roy M Anderson and Robert M May. *Infectious diseases of humans: dynamics and control*. Oxford university press, 1992.
- Yoshua Bengio, Aaron Courville, and Pascal Vincent. Representation learning: A review and new perspectives. *IEEE transactions on pattern analysis and machine intelligence*, 2013.
- Thierry Bertin-Mahieux, Daniel P.W. Ellis, Brian Whitman, and Paul Lamere. The million song dataset. In *Proceedings of the 12th International Conference on Music Information Retrieval*, 2011.
- Antoine Bordes, Nicolas Usunier, Alberto Garcia-Duran, Jason Weston, and Oksana Yakhnenko. Translating embeddings for modeling multi-relational data. *Advances in neural information processing systems*, 2013.
- Martin R Bridson and André Haefliger. *Metric spaces of non-positive curvature*, volume 319. Springer Science & Business Media, 2013.
- John Burkardt. Cities-city distance datasets. *URL https://rdrr. io/cran/TSP/man/USCA312. html*, 2011.
- Chen Cai, Dingkang Wang, and Yusu Wang. Graph coarsening with neural networks. In *International conference on machine learning*, 2021.
- Zongsheng Cao, Qianqian Xu, Zhiyong Yang, Xiaochun Cao, and Qingming Huang. Geometry interaction knowledge graph embeddings. In *Proceedings of the AAAI Conference on Artificial Intelligence*, volume 36, 2022.
- Ines Chami, Zhitao Ying, Christopher Ré, and Jure Leskovec. Hyperbolic graph convolutional neural networks. *Advances in neural information processing systems*, 2019.
- Ines Chami, Albert Gu, Vaggos Chatziafratis, and Christopher Ré. From trees to continuous embeddings and back: Hyperbolic hierarchical clustering. Advances in Neural Information Processing Systems, 2020a.
- Ines Chami, Adva Wolf, Da-Cheng Juan, Frederic Sala, Sujith Ravi, and Christopher Ré. Low-dimensional hyperbolic knowledge graph embeddings. In *Proceedings of the 58th Annual Meeting of the Association for Computational Linguistics*, pp. 6901–6914. Association for Computational Linguistics, 2020b.
- Ines Chami, Adva Wolf, Da-Cheng Juan, Frederic Sala, Sujith Ravi, and Christopher Ré. Low-dimensional hyperbolic knowledge graph embeddings. Association for Computational Linguistics, 2020c.
- Wouter de Nooy, Andrej Mrvar, and Vladimir Batagelj. Exploratory social network analysis with pajek: Revised and expanded second edition. *Cambridge: Cambridge University Press*, 2011.
- Mukund Deshpande and George Karypis. Item-based top-n recommendation algorithms. *ACM Transactions on Information Systems*, 2004.
- Tim Dettmers, Pasquale Minervini, Pontus Stenetorp, and Sebastian Riedel. Convolutional 2d knowledge graph embeddings. In *Proceedings of the AAAI conference on artificial intelligence*, 2018.
- Francesco Di Giovanni, Giulia Luise, and Michael Bronstein. Heterogeneous manifolds for curvature-aware graph embedding. *ICLR Workshop on Geometrical and Topological Representation Learning*, 2022.
- Lev Finkelstein, Evgeniy Gabrilovich, Yossi Matias, Ehud Rivlin, Zach Solan, Gadi Wolfman, and Eytan Ruppin. Placing search in context: The concept revisited. In *Proceedings of the 10th international conference on World Wide Web*, 2001.
- Albert Gu, Frederic Sala, Beliz Gunel, and Christopher Ré. Learning mixed-curvature representations in product spaces. In *International Conference on Learning Representations*, 2018.

- Xiangnan He, Tao Chen, Min-Yen Kan, and Xiao Chen. Trirank: Review-aware explainable recommendation by modeling aspects. In *Proceedings of the 24th ACM International on Conference on Information and Knowledge Management*, 2015.
- Cheng-Kang Hsieh, Longqi Yang, Yin Cui, Tsung-Yi Lin, Serge Belongie, and Deborah Estrin. Collaborative metric learning. In *Proceedings of the 26th international conference on world wide web*, 2017.
- Shaoxiong Ji, Shirui Pan, Erik Cambria, Pekka Marttinen, and S Yu Philip. A survey on knowledge graphs: Representation, acquisition, and applications. *IEEE transactions on neural networks and learning systems*, 2021.
- Matthias Leimeister and Benjamin J Wilson. Skip-gram word embeddings in hyperbolic space. *arXiv preprint arXiv:1809.01498*, 2018.
- Jianxin Li, Xingcheng Fu, Qingyun Sun, Cheng Ji, Jiajun Tan, Jia Wu, and Hao Peng. Curvature graph generative adversarial networks. 2022.
- Qi Liu, Maximilian Nickel, and Douwe Kiela. Hyperbolic graph neural networks. *Advances in Neural Information Processing Systems*, 2019.
- Yu Meng, Jiaxin Huang, Guangyuan Wang, Chao Zhang, Honglei Zhuang, Lance Kaplan, and Jiawei Han. Spherical text embedding. *Advances in Neural Information Processing Systems*, 2019.
- Tomas Mikolov, Kai Chen, Greg Corrado, and Jeffrey Dean. Efficient estimation of word representations in vector space. *International Conference on Learning Representations*, 2013.
- Maximillian Nickel and Douwe Kiela. Poincaré embeddings for learning hierarchical representations. Advances in neural information processing systems, 2017.
- Yann Ollivier. Ricci curvature of markov chains on metric spaces. *Journal of Functional Analysis*, 2009.
- Peter Petersen. Riemannian geometry. Springer, 2006.
- Ondrej Skopek, Octavian-Eugen Ganea, and Gary Bécigneul. Mixed-curvature variational autoencoders. In *International Conference on Learning Representations*, 2020.
- RP Sreejith, Karthikeyan Mohanraj, Jürgen Jost, Emil Saucan, and Areejit Samal. Forman curvature for complex networks. *Journal of Statistical Mechanics: Theory and Experiment*, 2016.
- Zhiqing Sun, Zhi-Hong Deng, Jian-Yun Nie, and Jian Tang. Rotate: Knowledge graph embedding by relational rotation in complex space. *International Conference on Learning Representations*, 2019.
- Jun Takeuchi, Noriki Nishida, and Hideki Nakayama. Neural networks in a product of hyperbolic spaces. In *Proceedings of the 2022 Conference of the North American Chapter of the Association for Computational Linguistics: Human Language Technologies*, 2022.
- Jake Topping, Francesco Di Giovanni, Benjamin Paul Chamberlain, Xiaowen Dong, and Michael M Bronstein. Understanding over-squashing and bottlenecks on graphs via curvature. In *International conference on machine learning*, 2022.
- Lucas Vinh Tran, Yi Tay, Shuai Zhang, Gao Cong, and Xiaoli Li. Hyperml: A boosting metric learning approach in hyperbolic space for recommender systems. In *Proceedings of the 13th International Conference on Web Search and Data Mining*, 2020.
- Duncan J Watts and Steven H Strogatz. Collective dynamics of 'small-world' networks. *nature*, 1998.
- Richard C Wilson, Edwin R Hancock, Elżbieta Pekalska, and Robert PW Duin. Spherical and hyperbolic embeddings of data. *IEEE transactions on pattern analysis and machine intelligence*, 2014.

- Yi Xu, Dongsheng Wang, Bo Chen, Ruiying Lu, Zhibin Duan, Mingyuan Zhou, et al. Hyperminer: Topic taxonomy mining with hyperbolic embedding. *Advances in Neural Information Processing Systems*, 35, 2022a.
- Zhirong Xu, Shiyang Wen, Junshan Wang, Guojun Liu, Liang Wang, Zhi Yang, Lei Ding, Yan Zhang, Di Zhang, Jian Xu, et al. Amcad: Adaptive mixed-curvature representation based advertisement retrieval system. In 2022 IEEE 38th International Conference on Data Engineering (ICDE), pp. 3439–3452. IEEE, 2022b.
- Zhitao Ying, Jiaxuan You, Christopher Morris, Xiang Ren, Will Hamilton, and Jure Leskovec. Hierarchical graph representation learning with differentiable pooling. *Advances in neural information processing systems*, 2018.
- Di You, Thanh Tran, and Kyumin Lee. Multi-behavior recommendation with hyperbolic geometry. In 2022 IEEE International Conference on Big Data (Big Data), pp. 1750–1759. IEEE, 2022.
- Tao Yu and Christopher De Sa. Random laplacian features for learning with hyperbolic space. In *International Conference on Learning Representations*, 2023.
- Shuai Zhang, Yi Tay, Wenqi Jiang, Da-cheng Juan, and Ce Zhang. Switch spaces: Learning product spaces with sparse gating. *arXiv preprint arXiv:2102.08688*, 2021.

# ADDITIONAL BACKGROUND

**Riemannian Geometry** Let  $\mathcal{M}^n$  be a smooth manifold in n-dimensional space, where  $\mathcal{M}^n$  is locally approximated by an n-dimensional Euclidean tangent space  $T_p\mathcal{M}$  at  $p\in\mathcal{M}$ . The pair  $(\mathcal{M}, g)$  is called a Riemannian manifold if  $\mathcal{M}$  is equipped with a positive-definite metric tensor g that satisfies certain conditions. Geodesics are the shortest-distance paths on manifolds, and the metric tensor g is integrated along the geodesic to compute distances on a Riemannian manifold. The exponential map  $\exp_p: T_p\mathcal{M} \to \mathcal{M}$  and logarithmic maps  $\log_p: \mathcal{M} \to T_p\mathcal{M}$  are two common bijections defined on the manifold  $\mathcal{M}$ . A formal introduction to Riemannian manifolds can be found in Petersen (2006).

**Product manifolds** Consider a sequence of smooth Riemannian manifolds  $\mathcal{M}_1, \mathcal{M}_2, \ldots, \mathcal{M}_k$ .  $\mathcal{M}_i$  can be positive (Spherical), zero (Euclidean), negative (Hyperbolic) curvature space. The product manifold is defined as the Cartesian product  $\mathcal{M} = \mathcal{M}_1 \times \mathcal{M}_2 \times \cdots \times \mathcal{M}_k$ . We write a point  $p \in \mathcal{M}$  through their coordinates  $p = (p_1, \ldots, p_k), p_i \in \mathcal{M}_i$ . Similarly, a tangent vector  $v \in T_p \mathcal{M}$  can be written as  $(v_1, \ldots, v_k) : v_i \in T_{p_i} \mathcal{M}_i$ . Gradient descent on manifolds requires the notion of taking steps. This step can be performed in the tangent space and transferred to the manifold via the logarithmic map, and exponential map Petersen (2006). The product space is also equipped with a distance function. The squared distance between points  $x, y \in \mathcal{M}$  is defined as:  $d_P^2(x,y) = \sum_{i=1}^k d_i^2(x_i, y_i).$ 

#### В CURVATURE ESTIMATION ON GRAPH DATA

**Curvature estimation on simple graphs** There are three commonly used definitions for local graph curvature: Ollivier-Ricci Ollivier (2009), Forman-Ricci Sreejith et al. (2016), and sectional curvature Gu et al. (2018). In this paper, we use sectional curvature for estimating the geometric structures of graphs. Sectional curvature is determined by geometric triangle properties as follows.

**Theorem 1:** Recall from Gu et al. (2018) that on a given constant curvature geometric space, if abc is a geodesic triangle and m is the midpoint of bc, then  $d(a,m)^2 + \frac{d(b,c)^2}{4} - \frac{d(a,b)^2 + d(a,c)^2}{2}$  is equal to zero when the underlying space is Euclidean, is positive in spherical and negative in hyperbolic space, respectively.

*Proof:* We provide proof of Theorem 1.

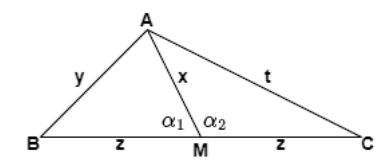


Figure 3: Geodesic triangle visualization.

$$A = d(a,m)^{2} + \frac{d(b,c)^{2}}{4} - \frac{d(a,b)^{2} + d(a,c)^{2}}{2}$$
(7)

$$=x^2+z^2-\frac{y^2}{2}-\frac{t^2}{2}\tag{8}$$

$$= \frac{1}{2}(2x^2 + 2z^2 - y^2 - t^2) \tag{9}$$

$$2 2$$

$$= \frac{1}{2}(2x^2 + 2z^2 - y^2 - t^2) (9)$$

$$= \frac{1}{2}[(x^2 + z^2 - y^2) + (x^2 + z^2 - t^2)] (10)$$

$$= \frac{1}{2}[2xz\cos\alpha_1 + 2xz\cos\alpha_2] (11)$$

$$= \frac{1}{2} [2xz\cos\alpha_1 + 2xz\cos\alpha_2] \tag{11}$$

$$=xz(\cos\alpha_1+\cos\alpha_2)\tag{12}$$

Table 7: Statistics of all four synthetic datasets.

Dataset	#Nodes $( V )$	#Edges ( $ E $ )
Tree	40	39
Cycle	40	40
Circle of tree	40	40

From Equation (6), we apply the cosine rule <sup>1</sup>. We have three cases:

- $\cos \alpha_1 + \cos \alpha_2 = 0$ :  $\alpha_1$  and  $\alpha_2$  are two supplementary angles,  $\alpha_1 + \alpha_2 = 180^0$ . Then the triangle is in Euclidean space.
- Similarly, it will be negative in hyperbolic and positive in the spherical curvature space.

Curvature estimation on graph data Given theorem (1), let v be a node in G; b, c neighbors of v and a any other node. Then, the sectional curvature of a node v and its neighbors b, c is defined following:  $\frac{1}{|V|-3} \sum_{a \in G \setminus \{v,b,c\}} \xi_G(v;b,c;a)$  where

$$\xi_G(v;b,c;a) = \frac{1}{2d_G(a,v)} \left( d_G(a,v)^2 + \frac{d_G(b,c)^2}{4} - \frac{d_G(a,b)^2 + d_G(a,c)^2}{2} \right)$$
(13)

and  $2d_G(v; b, c)$  is included to yield the right scalings for trees and cycles.

Next, we estimate the curvature of some typical topology graph structures. Star  $\mathbf{S}_n$  is created from one central node and n leaves. We consider  $n \geq 3$ , the local curvature at the center node v with two neighbors b,c is -1. Tree  $\mathbf{T}_b$  with branching factor b is the finite depth tree with  $b \geq 2$ . The sectional curvature on the tree in the range  $\xi(T) \in [-1,0]$ . Cycles graph  $\mathbf{C}_n$  with  $n \geq 4$ . If n is even, then  $\xi_{C_n}(v;b,c;a)=0$  for all points except the one diametrically opposite to v for which have  $\xi_{C_n}(v;b,c;a)=1$ . If n is odd, then for two points we have  $\xi_{C_n}(v;b,c;a)=\frac{n}{2(n-1)}$ . As a result,  $\xi(C_n)=\frac{1}{n-3}$  for even n and  $\xi(C_n)=\frac{n}{(n-1)(n-3)}$  for odd n.

**Distortion error on simple graphs** We have demonstrated the limitations of using a single curvature approach to embed graphs with varying topologies. To investigate the impact of curvature spaces on the quality of embedding spaces, we conducted experiments on three synthetic datasets with specific structures, including trees, circles, and rings of trees (Table 7). Figure 4 shows the distortion error results for Cycle and Tree graphs. Our findings suggest that different graph structures require corresponding curvature spaces for optimal embedding quality. For instance, spherical space (positive curvature) provides the least distortion error for cycle-like datasets (from  $\mathbf{S}_3$  to  $\mathbf{S}_{50}$ ), while hyperbolic spaces (negative curvature) give a minimal error for tree-like datasets (from  $\mathbf{H}_3$  to  $\mathbf{H}_{50}$ ). All three models show some advancements compared to others in certain cases. However, the overall distortions achieved are significantly higher than when using hyperbolic space with tree-like or spherical space with circle-like data. For example, the distortion error on the Cycle tree is 0.09 compared to 0.02 on  $\mathbf{H}_{10}$  with Cycle data and 0.042 on  $\mathbf{S}_5$  with simple Tree data. Therefore, using a product of individual spaces can improve the accuracy of embedding data with a mixture of structures.

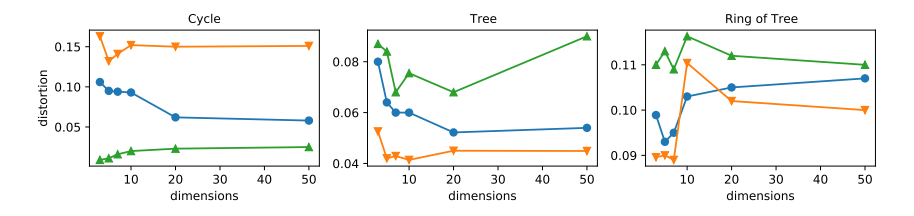


Figure 4: Comparison of using single spaces in Cycle and Tree data sets when gradually increasing the number of dimensions. Blue is Euclidean, Orange is Hyperbolic and Green is Spherical.

<sup>&</sup>lt;sup>1</sup>https://en.wikipedia.org/wiki/Law\_of\_cosines

# C ADDITIONAL EXPERIMENTAL RESULTS

#### C.1 Graph reconstruction task

**Datasets** The synthetic datasets we use are small graphs with 40 nodes that are designed to have specific geometric structures, including a circle, a tree, and a ring of trees. To assess the effectiveness of our approach on larger and more complex graphs, we also use three benchmark datasets: CsPhD de Nooy et al. (2011), Power Watts & Strogatz (1998), and Cities Burkardt (2011). The Cities dataset consists of 1025 nodes and 1043 edges, while the Power dataset contains 4941 nodes and 6594 edges. Additionally, the CsPhD dataset has 312 nodes and 48516 edges.

**Baselines** We compare the distortion error of node embeddings on both synthetic and benchmark datasets between our proposed model and the product spaces (PM) Gu et al. (2018) method.

**Metrics** We use two standard metrics to measure the quality of embeddings: average distortion  $D_{\mathrm{avg}}$  and mean average precision mAP.  $D_{\mathrm{avg}}$  is a global metric that considers all the exact distance values. Let G=(V,E) be a graph and node  $a\in V$  have a neighborhood  $\mathcal{N}_a=b_1,\cdots,b_{\deg(a)},$  where  $\deg(a)$  is the degree of a. In the embedding f, define  $R_{a,b_i}$  to be the smallest ball around f(a) that contains  $b_i$ , which means  $R_{a,b_i}$  is the smallest set of nearest points required to retrieve the  $i^{\mathrm{th}}$  neighbor of a in f. Thus,  $mAP=\frac{1}{|V|}\sum_{a\in V}\frac{1}{\deg(a)}\sum_{i=1}^{|\mathcal{N}a|}\frac{|\mathcal{N}a\cap R_{a,b_i}|}{|R_{a,b_i}|}$ . mAP is a ranking-based measure for local neighborhoods, and it does not track exact distances like  $D_{\mathrm{avg}}$ .

Table 8: Average distortion  $D_{\text{avg}}(\downarrow)$  and mAP ( $\uparrow$ ) on CsPhDs and Power datasets on dimensions 10 and 50 respectively. The best  $D_{\text{avg}}$  results are in boldface, while the second best results are underlined.

Method	Models	Cs P	hDs	Pov	ver
		$D_{\text{avg}}$	mAP	$D_{\mathrm{avg}}$	mAP
PM	$(\mathbb{H}^2)^5$	0.0357	0.9694	0.0396	0.8739
	$(\mathbb{H}^5)^2$	0.0382	0.9628	0.0365	0.8605
	$(\mathbb{S}^5)^2$	0.0579	0.7940	0.0471	0.8059
	$\stackrel{(\mathbb{H}^5)^2}{(\mathbb{S}^5)^2} \ \stackrel{(\mathbb{S}^2)^5}{(\mathbb{S}^2)^5}$	0.0562	0.8314	0.0483	0.8818
	$\mathbb{H}^5 imes\mathbb{S}^5$	0.0529	0.9041	0.0323	0.8850
WEIGHTED-PM					
	$\mathbf{s}(\mathbb{H}^2)^5$	0.0301	0.9699	0.0423	0.8540
		(+15.6%)			
	$\mathbf{s}(\mathbb{H}^5)^2$	0.0489	0.8465	0.034	0.88
	$egin{array}{c} \mathbf{s}(\mathbb{H}^5)^2 \ \mathbf{s}(\mathbb{S}^5)^2 \ \mathbf{s}(\mathbb{S}^2)^5 \end{array}$	0.056	0.813	0.0431	0.812
	$\mathbf{s}(\mathbb{S}^2)^5$	0.055	0.8361	0.0402	0.894
	$\mathbf{s}_1\mathbb{H}^5 imes\mathbf{s}_2\mathbb{S}^5$	0.0494	0.9231	0.0231	0.8842
				(+28.4%)	
PM	(10) 5				
	$(\mathbb{H}^{10})^5$	0.0657	0.913	0.0501	0.869
	$(\mathbb{H}^5)^{10}$	0.0786	0.8600	0.0723	0.842
	$(\mathbb{H}^{5})^{10}$ $(\mathbb{S}^{10})^{5}$ $(\mathbb{S}^{5})^{10}$	0.0726	0.843	0.0682	0.84
	$(S^5)^{10}$	0.07	0.89	0.0701	0.831
	$(\mathbb{H}^{10})^3 \times (\mathbb{S}^{10})^2$	0.0620	0.9120	0.0510	0.8500
	$(\mathbb{H}^{10})^2 \times (\mathbb{S}^{10})^2 \times \mathbb{E}^{10}$	0.0571	0.9071	0.0495	0.8561
WEIGHTED-PM	(==10) F				
	$\mathbf{s}(\mathbb{H}^{10})^5$	0.062	0.932	0.0479	0.871
	$\mathbf{s}(\mathbb{H}^5)^{10}$	0.0591	0.8900	0.0503	0.8570
	$\mathbf{s}(\mathbb{H}^{10})^5 \ \mathbf{s}(\mathbb{H}^5)^{10} \ \mathbf{s}(\mathbb{S}^{10})^5 \ \mathbf{s}(\mathbb{S}^5)^{10}$	0.074	0.829	0.0613	0.86
	$\mathbf{s}(\mathbb{S}^5)^{10}$	0.062	0.87	0.0648	0.871
	$\mathbf{s_1}(\mathbb{H}^{10})^3 imes\mathbf{s_2}(\mathbb{S}^{10})^2$	0.0590	0.9312	0.0426	0.8620
	(mm10) 2 (m10) 2 —10			(+13.9%)	
	$\mathbf{s_1}(\mathbb{H}^{10})^2  imes \mathbf{s_2}(\mathbb{S}^{10})^2  imes \mathbf{s}_3 \mathbb{E}^{10}$	0.0460	0.9240	0.0502	0.8600
		(+19.3%)			

Table 9: Statistics the number of entities, relations, and training, validations, and test triplets for two datasets.

Dataset	#entity	#relation	#training	#validation	#test
FB15k-237	14,541	1,345	272,115	17,535	20,466
WN18RR	40,943	11	86,835	3,034	3,134

#### C.2 ADDITIONAL INFORMATION FOR RECOMMENDATION TASK

**Metrics** We use two measures *Hit Ratio* (H) Deshpande & Karypis (2004) and *Normalized Discounted Cumulative Gain* (N) He et al. (2015) to examine the predictive ability of these models. The final H@k and N@k are averaged on all users' H@k and N@k scores. We choose k=10 to evaluate the model.

**Datasets** We perform experiments on two popular datasets, MovieLens-1M and LastFM-20K. The LastFm dataset (Bertin-Mahieux et al., 2011) is obtained from a music website<sup>2</sup>. It is preprocessed to have 1892 users and 17632 music records. The MovieLens-1M is created from 6040 users and 3706 movies.

**Baselines** We consider the three works below as the baselines for our model: CML Hsieh et al. (2017), HyperML Vinh Tran et al. (2020). For specific, CML Hsieh et al. (2017) investigates the relationship between metric learning and collaborative filtering. It proposes a method that learns a joint metric space capable of encoding not only users' preferences but also the similarity between users and items. HyperML Vinh Tran et al. (2020) presents the connection between metric learning in hyperbolic space and collaborative filtering by exploring hyperbolic geometry. HyperML-PM is our extension of HyperML in the product of model space. HyperML-WPM (Our) is our extension of HyperML in the product of model spaces with the gating mechanism.

#### C.3 ADDITIONAL INFORMATION FOR KNOWLEDGE GRAPH EMBEDDING

**Metrics** The performance of various models is evaluated using two standard metrics: mean reciprocal rank (MRR) and hit rate (HR@3).

**Datasets** We used two standard datasets, WN18RR Dettmers et al. (2018) and FB15K-237 Bordes et al. (2013), for our analysis. WN18RR is derived from WordNet, a lexical database of semantic relations between words. FB15K-237 is a subset of the Freebase knowledge graph, which is a comprehensive resource containing general information. Table 9 shows the statistics of the two datasets.

**Objective function** Given a knowledge graph  $\mathcal{G}$  with a set of entities  $\mathcal{E}$  and a set of relation  $\mathcal{R}$ . Each triplet  $(h, r, t) \in \mathcal{G}$  is included by head entity h, tail entity t, and the relation  $r \in \mathcal{R}$  between them.

There are a lot of works that propose RotE Sun et al. (2019) in Euclidean space, and RotH Chami et al. (2020b) in Hyperbolic space. In this work, we extend to the product of different curvature spaces. Formally, entities h,t are represented by vector  $\mathbf{e}_h,\mathbf{e}_t\in\mathbb{R}^b$  and the relation r is represented by two translation vectors  $\alpha_r,\beta_r\in\mathbb{R}^b$  and a rotation vector  $\gamma_r\in\mathbb{R}^b$ . The head entity will translate twice via Mobius addition operation and rotate one time.

$$Q(h,r) = \operatorname{Rot}(\exp_0^c(\mathbf{e}_h) \oplus_c \exp_0^c(\alpha_r), \gamma_r) \oplus_c \exp_0^c(\beta_r)$$
(14)

with c>0 and  $\exp_0^c$  is the exponential map over the origin. Rot is a rotation function with  $\gamma_r$  is the rotation matrix.

According to the above definition, for each triple (h, r, t), we define the distance function as:

$$d_r(h,t) = \sqrt{d_{\mathcal{M}_c}^2(Q(h,r), \exp_0^c(\mathbf{e}_t))}$$
(15)

<sup>&</sup>lt;sup>2</sup>http://millionsongdataset.com/lastfm/

Table 10: Benchmark's statistic for Node Classification and Link Prediction tasks.

Dataset	#Nodes	#Edges	#Classes	$\delta$
DISEASE	1044	1043	2	0
AIRPORT	3188	18631	4	1

where  $\mathcal{M}_c$  is the product of curvature manifold. In Sun et al. (2019), the distance function of RotatE for the triple (h, r, t) is defined as:  $d_r(h, r) = ||h \odot r - t||$ 

The final negative sampling loss is defined by the cross-entropy loss:

$$\mathcal{L} = \sum_{(h,r,t)\in\Omega} \log(1 + \exp(-Y_{(h,r,t)}d_r(h,t)))$$
 (16)

where  $Y_{(h,r,t)} \in \{1, -1\}$  is a binary label indicating whether a triplet is real or not.

**Baselines** RotatE Sun et al. (2019) is a knowledge graph embedding that is used to learn the representations of entities and relations in knowledge graphs. RotatH is the extension of RotatE Sun et al. (2019) in the hyperbolic space. Product-RotatH is the extension of RotatE in the product of the hyperbolic spaces Takeuchi et al. (2022). SwisE Zhang et al. (2021) used the gating mechanism which is learned to choose the component space for knowledge graph embedding. WEIGHTED-PM-Rotat is our extension by using the product of manifold in representing the relations among entities in the knowledge graph.

#### C.4 ADDITIONAL INFORMATION FOR NODE CLASSIFICATION AND LINK PREDICTION

**Metrics** We utilize ROC AUC as a metric to evaluate the performance of Link Prediction (LP), whereas we rely on the F1 score to assess the Node Classification (NC) performance. In both cases, a higher score indicates better performance.

**Datasets** In this experiment, we evaluate model performance on the two different benchmark datasets. DISEASE is the dataset of Infectious diseases from Oxford University Anderson & May (1992). AIRPORT: is the dataset of airline routes from OpenFlight.org. Each node represents an airport, and the edge represents airline routes among these airports. Detailed information regarding these datasets is provided in Table 10.

**Baselines** We evaluate the contributions of our proposed model by measuring the F1 and AUC scores on two datasets, compared with five different baseline models: MLP and Hyperbolic-MLP are two variants of multilayer perceptron (MLP) classifiers operating on the Euclidean (E) and hyperbolic space (H), respectively. HGCN Chami et al. (2019) is an extension of graph convolutional networks (GCNs) to hyperbolic geometry. Product-HGCN Takeuchi et al. (2022) extends GCNs in the product of hyperbolic geometries. Mix-GCN Gu et al. (2018) extends GCNs in the product of hyperbolic, spherical, and Euclidean spaces. Our proposed model (WEIGHTED-PM-GCN) extends GCNs with a gating mechanism in the product of different curvature spaces (H, E, S).